HUMAN GENE THERAPY CLINICAL DEVELOPMENT 25:164–177 (September 2014)

DOI: 10.1089/humc.2013.239

Research Articles

Comparative Efficacy and Safety of Multiple Routes of Direct CNS Administration of Adeno-Associated Virus Gene Transfer Vector Serotype rh.10 Expressing the Human Arylsulfatase A cDNA to Nonhuman Primates

Jonathan B. Rosenberg,[1] Dolan Sondhi,[1] David G. Rubin,[1] Sébastien Monette,[2] Alvin Chen,[1] Sara Cram,[1] Bishnu P. De,[1] Stephen M. Kaminsky,[1] Caroline Sevin,[3,4] Patrick Aubourg,[3,4] and Ronald G. Crystal[1]

Abstract

Metachromatic leukodystrophy (MLD), a fatal disorder caused by deficiency of the lysosomal enzyme arylsulfatase A (ARSA), is associated with an accumulation of sulfatides, causing widespread demyelination in both central and peripheral nervous systems. On the basis of prior studies demonstrating that adeno-associated virus AAVrh.10 can mediate widespread distribution in the CNS of a secreted lysosomal transgene, and as a prelude to human trials, we comparatively assessed the optimal CNS delivery route of an AAVrh.10 vector encoding human ARSA in a large animal model for broadest distribution of ARSA enzyme. Five routes were tested (each total dose, 1.5×10^{12} genome copies of AAVrh.10hARSA-FLAG): (1) delivery to white matter centrum ovale; (2) deep gray matter delivery (putamen, thalamus, and caudate) plus overlying white matter; (3) convection-enhanced delivery to same deep gray matter locations; (4) lateral cerebral ventricle; and (5) intraarterial delivery with hyperosmotic mannitol to the middle cerebral artery. After 13 weeks, the distribution of ARSA activity subsequent to each of the three direct intraparenchymal administration routes was significantly higher than in phosphate-buffered saline-administered controls, but administration by the intraventricular and intraarterial routes failed to demonstrate measurable levels above controls. Immunohistochemical staining in the cortex, white matter, deep gray matter of the striatum, thalamus, choroid plexus, and spinal cord dorsal root ganglions confirmed these results. Of the five routes studied, administration to the white matter generated the broadest distribution of ARSA, with 80% of the brain displaying more than a therapeutic (10%) increase in ARSA activity above PBS controls. No significant toxicity was observed with any delivery route as measured by safety parameters, although some inflammatory changes were seen by histopathology. We conclude that AAVrh.10-mediated delivery of ARSA via CNS administration into the white matter is likely to be safe and yields the widest distribution of ARSA, making it the most suitable route of vector delivery.

Introduction

Metachromatic leukodystrophy (MLD) is a rare, autosomal recessive lysosomal storage disorder caused by mutations in the lysosomal enzyme arylsulfatase A (ARSA) gene (von Figura *et al.*, 2001; Aubourg *et al.*, 2011; Batzios and Zafeiriou, 2012). Historically, MLD is classified by age of onset: the late infantile form is most common, with the less common presentations in juveniles or adults (Gieselmann and Krageloh-Mann, 2010; Aubourg *et al.*, 2011). The estimated incidence of the disease ranges from 1 in 43,000 to 1 in 70,000 live births (Aubourg *et al.*, 2011; Patil and Maegawa, 2013). In most cases the prognosis is poor; in the late infantile form, the disease leads to a vegetative stage or death within 12 to 18 months of initial diagnosis (von Figura *et al.*, 2001). The

[1]Department of Genetic Medicine, Weill Medical College of Cornell University, New York, NY 10065.
[2]Tri-Institutional Laboratory of Comparative Pathology, Weill Cornell Medical College, Memorial Sloan-Kettering Cancer Center, and Rockefeller University, New York, NY 10065.
[3]INSERM U986, University Paris-Descartes, 75005 Paris, France.
[4]Neuropediatrics Unit, Bicêtre Hospital, Le Kremlin Bicêtre, 94275 Paris, France.

loss of functional ARSA enzyme leads to an accumulation of 3-*O*-sulfogalactosyl ceramides (sulfatides) in oligodendrocytes, myelin sheaths, and Schwann cells, triggering widespread demyelination in the CNS and peripheral nervous system (PNS) (Gieselmann *et al.*, 2003; Molander-Melin *et al.*, 2004; Takahashi and Suzuki, 2012; Patil and Maegawa, 2013). Sulfatides also accumulate in neurons, promoting neuronal dysfunction and degeneration (Gieselmann *et al.*, 2003; Molander-Melin *et al.*, 2004; Wittke *et al.*, 2004; Sevin *et al.*, 2007). As glial cells and neurons are highly sensitive to this aberrant storage, these cells are progressively lost, resulting in broad and rapid neurologic decline that manifests as ataxia, inability to walk or stand, seizures, and cognitive decline (von Figura *et al.*, 2001; Rauschka *et al.*, 2006; Gieselmann and Krageloh-Mann, 2010).

There are no proven treatments for MLD (Batzios and Zafeiriou, 2012; Patil and Maegawa, 2013; Miranda *et al.*, 2013). Because the disease affects all regions of the nervous system, treatment must reestablish the missing enzymatic function throughout (Beck, 2007; Gray, 2013). Because the blood–brain barrier prevents effective therapy with systemic administration of ARSA, investigators have explored the use of gene therapy to provide the missing ARSA enzyme in MLD via direct intraparenchymal administration or by the use of genetically modified bone marrow stem cells that differentiate into microglial cells in the CNS (Matzner *et al.*, 2000; Biffi *et al.*, 2004, 2006, 2013; Sevin *et al.*, 2006, 2007; Colle *et al.*, 2010; Piguet *et al.*, 2012). The CNS manifestations of MLD are ideal for a CNS gene therapy approach because the ARSA enzyme is secreted into the extracellular matrix and incorporated into neighboring and distant cells via the ubiquitous cell surface, mannose 6-phosphate (M6P) receptor (Willingham *et al.*, 1981; Funk *et al.*, 1992; Ghosh *et al.*, 2003). Normal mechanisms for secretion of ARSA enzyme, the process of retrograde transport via axonal connections, and the M6P scavenger system can be leveraged to deliver the ARSA enzyme to many more cells in the CNS than those transduced with the ARSA cDNA. This is especially important because oligodendrocytes that are affected by the lack of functional ARSA enzyme are not effectively transduced *in vivo* by most gene therapy vectors, including most serotypes of adeno-associated virus (AAV) (Colle *et al.*, 2010; Gieselmann and Krageloh-Mann, 2010). Comparisons of genotype and phenotype suggest that levels of enzyme 5–10% of normal are associated with a less severe form of the disease with delayed age of onset in adulthood and mortality (von Figura *et al.*, 2001; Rauschka *et al.*, 2006). Thus, the most severe phenotype of MLD should be ameliorated if ARSA enzyme levels of >5–10% normal can be achieved throughout the CNS.

As a vector strategy, we have used the AAVrh.10 rhesus-derived adeno-associated virus gene transfer vector to deliver normal human ARSA cDNA to the CNS of nonhuman primates. This study explores several delivery modalities (intraparenchymal, intraventricular, intraarterial) to determine the route and/or site of infusion that achieves the widest spread and persistence of ARSA expression in the CNS. Finally, using conventional toxicology assays, we assessed the safety of the best route of delivery as a step toward clinical development.

Results

The focus of this study was to identify the optimal means of delivering an AAVrh.10 vector encoding the normal human ARSA cDNA (AAVrh.10hARSA-FLAG) in order to achieve the widest distribution of transgene product as the next step toward translation to a clinical study. To do so we compared the current vector administration method used in gene therapy clinical trials for the late infantile neuronal ceroid lipofuscinosis (LINCL) clinical study (Worgall *et al.*, 2008; Souweidane *et al.*, 2010) with four alternative protocols, focusing on ARSA distribution and safety in African green monkeys. In the LINCL clinical trial, we administered the AAVrh.10 vector encoding the gene of interest, *CLN2*, to the white matter underlying the cerebral cortex, using stereotactic delivery, to six symmetrically distributed sites in both hemispheres at various depths through each burr hole (Worgall *et al.*, 2008; Souweidane *et al.*, 2010). In the present study we have compared this delivery scheme with delivery to the deep gray matter (via three sites per hemisphere), and assessed the impact of convection-enhanced delivery infusions into these gray matter sites (Supplementary Fig. S1; supplementary data are available online at www.liebertpub.com/humc). In addition, we assessed the potential of more vascular methods by delivery of the AAV vector into the lateral ventricle and via intraarterial delivery (Table 1).

Detection of ARSA-FLAG

To assess the distribution of vector-mediated ARSA expression above the background of endogenous ARSA, the AAV vector was designed to encode a biologically active ARSA protein tagged with a FLAG peptide. At sacrifice, day 91 after vector administration, the brain was excised and bisected into hemispheres, with the left hemisphere used for histopathological and immunohistochemical analysis and the right used for ARSA enzymatic analysis (Table 1). To quantify the extent of ARSA distribution across the brains, a subset of coronal slices (25% per brain) was analyzed by anti-FLAG immunohistochemistry. These slices were selected because of their proximity to the site of vector administration in order to visualize the distribution of vector-mediated ARSA transgene expression (FLAG-tagged). No FLAG expression was observed in the brains from the PBS control group (Fig. 1A–D). The brains from the three CNS intraparenchymal administration groups showed, to a variable degree, areas of ARSA-FLAG expression in various regions of white matter and gray matter, and occasional milder staining of the ependymal cells of the choroid plexus in the ventricles (Figs. 1 and 2). On the basis of the morphology of the cells, there were abundant neurons displaying positive ARSA-FLAG expression in the cortical regions (Fig. 1E, G–I, K, M, and P) and deep gray matter (Fig. 2E–G, I, J, and N). Similarly, on the basis of morphology, there were positive glial cells (Fig. 1E–G and J and Fig. 2H, L, and P).

While the vector was administered to the centrum semiovale white matter tracts, this route of vector delivery clearly demonstrated ARSA expression near the loci of the original deposits and far beyond in many deeper structures. As expected, ARSA protein was detected in the white matter tracts and cerebral cortical areas surrounding the injection

TABLE 1. STUDY DESIGN[a]

Treatment route	*Target site(s)*	*No. of sites/no. of deposits*	*Vector*[b]
White matter[c]	Centrum semiovale	6 sites/12 infusions	None (PBS)
	Centrum semiovale	6 sites/12 infusions	AAVrh.10hARSA-FLAG
Deep gray matter plus overlying white matter[d]	Caudate, putamen, thalamus plus overlying white matter (centrum semiovale)	6 sites/12 infusions	AAVrh.10hARSA-FLAG
Deep gray matter with convection-enhanced delivery[e]	Caudate, putamen, thalamus	6 sites/6 infusions	AAVrh.10hARSA-FLAG
Intraventricular[f]	Right lateral ventricle	1 site/1 infusion	AAVrh.10hARSA-FLAG
Intraarterial with mannitol pretreatment[g]	Middle cerebral artery branch (right side)	1 site/1 infusion	AAVrh.10hARSA-FLAG

[a]All nonhuman primates in the study were monitored for changes in behavior, anti-AAV neutralizing antibodies, serum chemistries, and complete blood counts at two time points presurgery, on the day of surgery (day 0), and on days 2, 7, 14, 28, 56, and 91 postsurgery as part of postsurgery surveillance. All nonhuman primates were killed 13 weeks postsurgery (day 91 ± 2 days), and the brain and spinal cord segments with adjacent dorsal root ganglia were excised to examine the extent of transgene enzymatic activity across the CNS and PNS.

[b]The total dose administered to each nonhuman primate receiving AAVrh.10hARSA-FLAG was 1.5×10^{12} genome copies irrespective of the route of delivery.

[c]White matter administration ($n = 4$, 2 with PBS and 2 with AAVrh.10hARSA-FLAG): Vector was administered in 12 locations via 2 frontal lobe burr holes (anterior and posterior) and 1 parietal burr hole per hemisphere; there were 2 locations per burr hole at different depths and 15 μl was deposited per location (rate, 1 μl/min).

[d]Deep gray matter with overlying white matter administration ($n = 2$ with AAVrh.10hARSA-FLAG): Vector was administered in 12 locations targeting the putamen, thalamus, and caudate, plus overlying white matter deposits in each hemisphere, 15 μl per location (rate, 1 μl/min).

[e]Deep gray matter administration using convection-enhanced delivery ($n = 2$ with AAVrh.10hARSA-FLAG): Vector was administered in six locations targeting the putamen, thalamus, and caudate in each hemisphere, with 50 μl per location (rates were ramped every 5 min from 1 to 3 μl/min at 0.5 μl/min).

[f]Intraventricular treatment ($n = 2$ with AAVrh.10hARSA-FLAG): Vector (75 μl) was administered into the frontal horn of the right lateral ventricle (rate, 15 μl/min).

[g]Intraarterial administration ($n = 1$ with AAVrh.10hARSA-FLAG): After use of mannitol (12 ml) to disrupt the blood–brain barrier, vector was administered into the major brain arterial supply (right middle cerebral artery branch) via a neonatal French catheter (1.2F).

sites. In addition, ARSA expression was observed in deep gray structures such as the septohippocampal nucleus, ventral posterior lateral nucleus of thalamus, caudate nucleus, putamen, and claustrum (Fig. 2), suggesting that enzyme spread may not be due to simple diffusion of ARSA, but may have resulted from vector and/or ARSA anterograde/retrograde transport in the CNS. Similar widespread results were observed when we targeted the deeper substructures of the CNS, such as the striatum and thalamus, by the deep gray matter with overlying white matter route. Beyond the expected staining in the targeted areas of the cerebral white matter and caudate nucleus, putamen, and thalamus, staining was observed to a lesser degree in the surrounding areas, such as the reticular nucleus of the thalamus, the globus pallidus (external segment; data not shown), and the insular cortex (granular field; data not shown). Compared with the intense staining observed for ARSA-FLAG by the white matter route, the deep gray matter with overlying white matter route overall had a lesser degree of staining outside of the directly targeted areas (putamen, caudate, and thalamus). The use of increased vector volume and the increased rate of delivery with the deep gray matter with the convection-enhanced delivery route resulted in ARSA expression more limited to the targeted and proximal areas (especially in the putamen). There was focal and intense staining of the caudate, putamen, and thalamus (Fig. 2), plus immediate surrounding areas, such as the internal capsule, reticular nucleus, claustrum, and anterior olfactory nucleus (data not shown). The degree of spread of ARSA across the CNS with the convection-enhanced delivery method was less than that observed for the white matter and deep gray matter with overlying white matter methods.

The brains from the group that received intraventricular delivery of AAVrh.10hARSA-FLAG showed only mild staining of the choroid plexus, without staining of gray or white matter (data not shown). Data from one animal in the intraarterial group did not show any staining for AAVrh.10hARSA-FLAG in the contralateral hemisphere (data not shown). On the basis of this detailed analysis, the white matter route of administration showed the largest spread of ARSA, as measured by FLAG staining in both white and gray matter, and appeared to be the best delivery route.

Histopathological examination of the brain revealed that all animals that received an intracerebral injection into the white matter or deep gray matter, including control (PBS-treated) animals, had mild focal meningeal histiocytic inflammation, superficial cortical atrophy and loss, and linear glial scars at the injection sites. These changes were likely due to physical injury by the needle, and in some cases by focal reactive bone growths that were compressing the cortex. All treated animals in the white matter, deep gray matter, and deep gray matter with convection-enhanced delivery groups had a well-demarcated area of lymphohistiocytic inflammation associated with each of the injection site (18 of 18 sites), affecting both white and gray matter. Most of these areas (13 of 18) also displayed white matter spongiosis (consistent with degeneration and loss), and gliosis. Histopathological evaluation of the coronal sections to determine the size of the white matter spongiosis and gliosis was used to evaluate the area of gliosis per total hemisphere transverse section area. When the areas of

FIG. 1. Comparison of detection of arylsulfatase A protein tagged with a FLAG peptide (ARSA-FLAG) in the cortical and white matter regions after intraparenchymal routes of vector delivery in nonhuman primate brains. Shown is immunohistochemistry from similar brain substructures in nonhuman primates administered AAVrh.10hARSA-FLAG via the white matter, deep gray matter with overlying white matter, and deep gray matter routes. The animals were killed 13 weeks postsurgery. Representative images from various brain substructures are displayed with areas of FLAG detection denoted by the brown staining, with blue indicating nuclei (hematoxylin counterstained). **(A–D)** Sections of a PBS control that received white matter administration. **(E–H)** AAVrh.10hARSA-FLAG via the white matter route. **(I–L)** AAVrh.10hARSA-FLAG via the deep gray matter with overlying white matter route. **(M–P)** AAVrh.10hARSA-FLAG via the deep gray matter with convection-enhanced delivery route. Cortical areas displayed represent sampling from lateral **(A, E, I,** and **M)** and medial **(C, G, K,** and **O)** cortical areas to demonstrate the spread of ARSA and/or vector. Locations of the sections shown (each labeled with the site) were identified with Nissl-stained coronal brain sections (http://brainmaps.org/). Scale bar (all panels), 50 μm.

degeneration were combined with section thickness, the percentage of cellular loss was only minor, 0.03–1.5% of the total brain. There was a strong correlation between the distribution of these lesions and the distribution of FLAG expression by immunohistochemistry. There was no trend in specific route or CNS targeted region and the degree of lesion observed.

Widespread detection of vector-mediated ARSA expression

To determine whether transgene ARSA expression was localized to the vicinity around the sites of administration or was widespread throughout the CNS, the CNS was analyzed for functional ARSA enzymatic activity in brain cubes, using a uniform grid as a reference. As expected, there was some variation in ARSA levels between the pairs of nonhuman primates used for each route, including the endogenous ARSA background levels in the PBS controls; therefore, the results reported are averaged expression levels for each surgical route of administration. Because nonhuman primates have native expression of ARSA, the PBS control monkeys ($n=2$) were used to define endogenous baseline ARSA levels in sham-treated African green monkeys. To determine the increase in ARSA expression due to vector administration in treated nonhuman primates relative to the endogenous baseline level, raw ARSA activity in brain cubes at corresponding locations in monkeys were averaged for each administration route ($n=2$ monkeys, except for the intraarterial group where $n=1$). The means were corrected by subtracting the mean activity of the corresponding PBS control brain cubes, and then expressed as the percent increase relative to the mean activity of the corresponding PBS cubes.

The increase in ARSA activity over endogenous baseline in the 1-cm^3 brain cubes is presented as a three-dimensional plot of cubes assembled into recreations of the right hemisphere of the nonhuman primate brains, where an increase of $>10\%$ ARSA activity is shown by blue-shaded cubes, $>25\%$ ARSA activity is shown by green-shaded cubes, and $>50\%$ ARSA activity is shown by red-shaded cubes (Fig. 3). This spatial representation demonstrated that ARSA activity was not only proximal to the site of vector administration, but spread well beyond these foci for the three CNS intraparenchymal routes. In contrast, such widespread ARSA activity was not seen with the intraventricular and intraarterial routes of delivery. With a limitation of $n=1$ for the intraarterial group, it remains unresolved whether the intraarterial method might have worked with different cerebral vascular routes. Both the white matter and deep gray matter with overlying white matter administration routes demonstrated widespread (laterally, rostrally, caudally, and ventrally from administration sites) expression of the ARSA transgene in the brains of treated NHPs. However, the white matter route results suggest a more consistent spread of ARSA activity compared with that of the other four methods. When the individual cube ARSA means were plotted the white matter route of vector administration provided the highest number of positive cubes, with ARSA levels $>50\%$ (31 cubes) compared with 19, 19, 3, and 0 cubes for the deep gray matter with overlying white matter, deep gray matter with convection-enhanced delivery, intraventricular, and intraarterial routes, respectively (Supplementary Fig. S2).

One goal of this study was to assess ARSA activity in the nonhuman primate CNS induced by AAVrh.10hARSA-FLAG administration at levels above the suggested therapeutic range (>5–10% normal). With this in mind we calculated the number and percentage of cubes that had ARSA levels that were 10, 25, and 50% greater than endogenous baseline levels in wild-type monkey brain (PBS controls). The highest increase in ARSA expression was with the white matter route of delivery, with 80, 61, and 32% of the cubes having levels that were greater than 10,

FIG. 2. Comparison of ARSA-FLAG detection in deep gray matter of the CNS after intraparenchymal routes of vector delivery in nonhuman primate brains. Shown is immunohistochemistry from similar brain substructures in nonhuman primates administered AAVrh.10hARSA-FLAG via the white matter, deep gray matter with overlying white matter, and deep gray matter routes. The animals were killed 13 weeks postsurgery. Representative images from various brain substructures are displayed with areas of FLAG detection denoted by the brown staining, with blue indicating nuclei (hematoxylin counterstained). **(A–D)** Sections of a PBS control that received white matter administration. **(E–H)** AAVrh.10hARSA-FLAG via the white matter route. **(I–L)** AAVrh.10hARSA-FLAG via the deep gray matter with overlying white matter route. **(M–P)** AAVrh.10hARSA-FLAG via the deep gray matter with convection-enhanced delivery route. Identification of brain substructures was made with Nissl-stained coronal brain sections (http://brainmaps.org/). Because the deep gray matter routes targeted the putamen and thalamus, these regions demonstrated higher concentrations of ARSA-FLAG vector and/or enzyme. Scale bar (all panels), 50 μm.

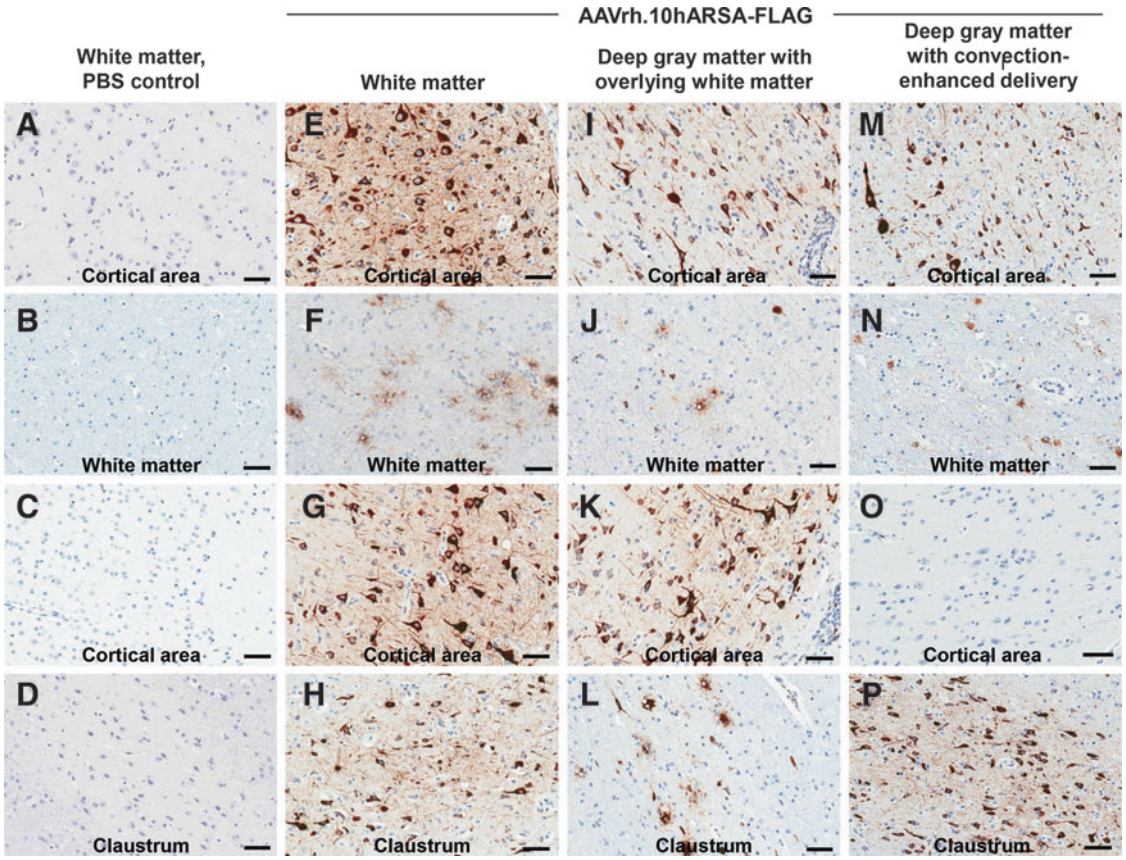
AAVrh.10hARSA-FLAG
White matter, PBS control
White matter
Deep gray matter with overlying white matter
Deep gray matter with convection-enhanced delivery
A
Cortical area
E
Cortical area
I
Cortical area
M
Cortical area
B
White matter
F
White matter
J
White matter
N
White matter
C
Cortical area
G
Cortical area
K
Cortical area
O
Cortical area
D
Claustrum
H
Claustrum
L
Claustrum
P
Claustrum

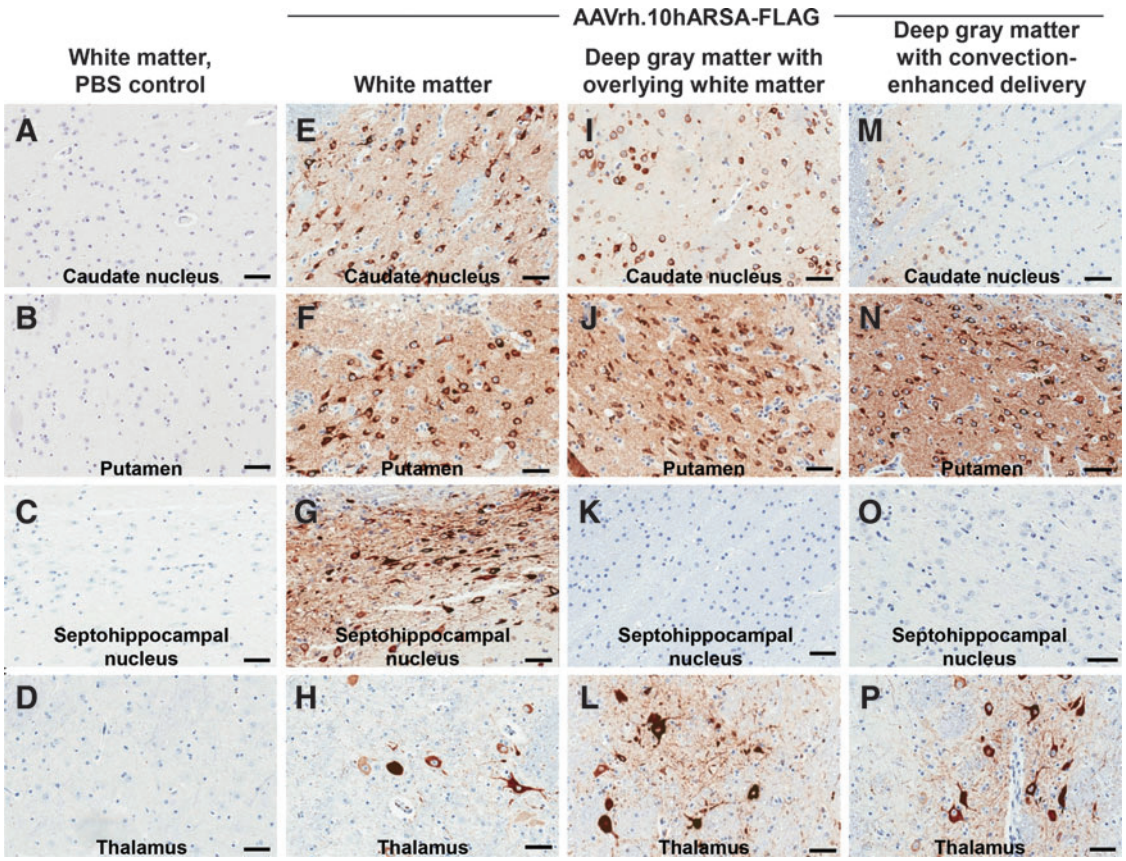
AAVrh.10hARSA-FLAG
White matter, PBS control
White matter
Deep gray matter with overlying white matter
Deep gray matter with convection-enhanced delivery
A
Caudate nucleus
E
Caudate nucleus
I
Caudate nucleus
M
Caudate nucleus
B
Putamen
F
Putamen
J
Putamen
N
Putamen
C
Septohippocampal nucleus
G
Septohippocampal nucleus
K
Septohippocampal nucleus
O
Septohippocampal nucleus
D
Thalamus
H
Thalamus
L
Thalamus
P
Thalamus

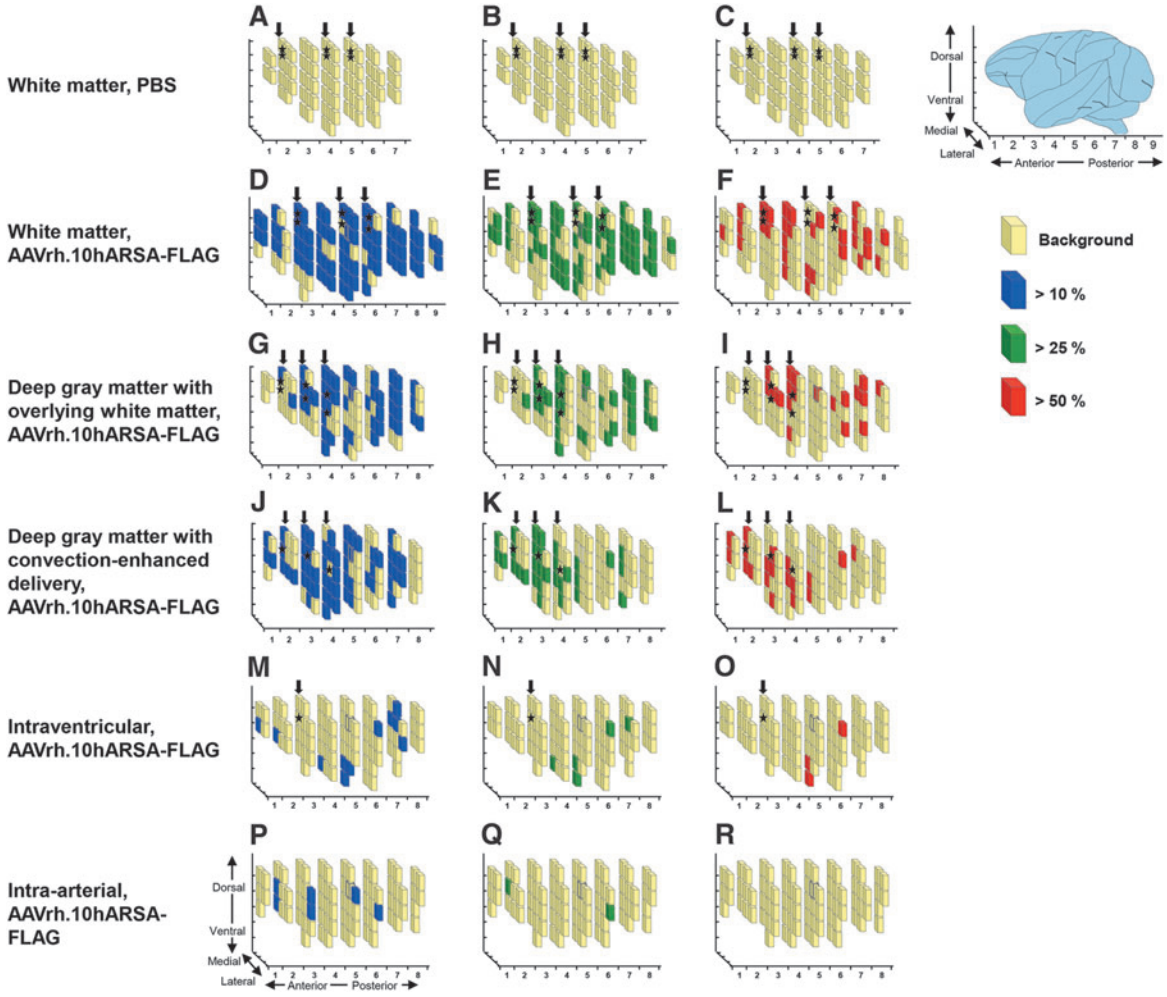

FIG. 3. Comparison of ARSA levels in AAVrh.10hARSA-FLAG-treated nonhuman primate CNS. The distribution of increase in ARSA transgene expression in the brains of nonhuman primates administered AAVrh.10hARSA-FLAG via the five surgical routes is represented by three-dimensional schematic drawings of the right hemispheres. African green monkeys ($n=11$) were administered AAVrh.10hARSA-FLAG (1.5×10^{12} genome copies [GC]) or PBS, as described in Table 1, and were killed 13 weeks postsurgery. Shown is the extent of ARSA distribution above wild-type background ARSA levels (determined from PBS-administered controls). Each primate brain was subdivided into $1\times1\times1$ cm (1-cm^3) cubes. The ARSA activity in cube lysates was determined by enzymatic conversion of the substrate *p*-nitrocatechol sulfate to 4-nitrocatechol, and expressed as nanomoles per minute per milligram of protein. The ARSA activity levels in corresponding brain cubes for each route ($n=2$ nonhuman primates [NHPs], except for the intraarterial route, for which there is no mean because $n=1$) were averaged and corrected by subtracting the corresponding PBS control brain cube mean, and then expressed as the percent increase relative to the corresponding PBS cube mean. Where a corresponding cube was lacking in the PBS control set, the global PBS mean (28.1 nmol/hr·mg, determined as the mean of all PBS cube sets) was used. In **(A–R)**, the light yellow cubes represent regions of background endogenous levels, blue cubes represent regions that had activity >10% endogenous levels, green cubes represent regions that had activity >25% endogenous levels, and red cubes represent regions that had activity >50% endogenous levels. **(A–C)** White matter administration route (PBS controls, $n=2$); **(D–F)** white matter administration route (AAVrh.10hARSA-FLAG, $n=2$); **(G–I)** deep gray matter with overlying white matter administration route (AAVrh.10hARSA-FLAG, $n=2$); **(J–L)** deep gray matter with convection-enhanced delivery (CED) (AAVrh.10hARSA-FLAG, $n=2$); **(M–O)** intraventricular administration route (AAVrh.10hARSA-FLAG, $n=2$); **(P–R)** intraarterial administration route (AAVrh.10hARSA-FLAG, $n=1$). *Left columns:* Cubes with >10% ARSA activity (blue). *Middle columns:* Cubes with >25% ARSA activity (green). *Right columns:* Cubes with >50% ARSA activity (red). Locations of the burr holes used for catheter placement are depicted by the vertical black arrows above each brain, with the approximate location of the sites of injection depicted by black stars. See Table 2 for percentage and number of brain cubes with >50% ARSA activity for each route.

25, and 50% relative to the mean wild-type levels, respectively (Table 2). In contrast, the deep gray matter with overlying white matter route provided 58, 41, and 23% of cubes having with levels greater than 10, 25, and 50% relative to the mean wild-type levels, and the deep gray matter route with convection-enhanced delivery yielded 62, 36, and 21% of the cubes with levels greater than 10, 25, and 50% relative to the mean wild-type levels. These results suggest that the white matter route of administration was the preferred route of delivery among the five routes tested.

Table 2. Percentage of Brain Cubes with Increases in Arylsulfatase A Activity Levels Relative to Phosphate-Buffered Saline Controls in Treated Nonhuman Primate Brains[a–c]

Route, vector	Total cubes	Cubes with >10% ARSA activity[d]		Cubes with >25% ARSA activity[d]		Cubes with >50% ARSA activity[d]	
		No. of cubes	Percentage of cubes	No. of cubes	Percentage of cubes	No. of cubes	Percentage of cubes
White matter, none (PBS)	79	0	0	0	0	0	0
White matter, AAVrh.10hARSA-FLAG	97	78	80	59	61	31	32
Deep gray matter with overlying white matter, AAVrh.10hARSA-FLAG	83	48	58	34	41	19	23
Deep gray matter with convection-enhanced delivery, AAVrh.10hARSA-FLAG	89	55	62	32	36	19	21
Intraventricular, AAVrh.10hARSA-FLAG	83	11	13	5	6	3	4
Intraarterial, AAVrh.10hARSA-FLAG	77	6	8	2	3	0	0

ARSA-FLAG, arylsulfatase A protein tagged with a FLAG peptide; PBS, phosphate-buffered saline.

[a]Comparison of number of 1-cm^3 brain cubes that displayed increased ARSA activity for each of the five routes ($n=2$ per route, except for the intraarterial delivery route [$n=1$]; averaged data for each route are presented here).

[b]ARSA values were corrected by subtracting the mean of the paired matched brain cube sets of PBS control nonhuman primates from the mean of the identical matched cube set obtained by any given route, and then expressed as the percent increase above the PBS mean corresponding to that cube set.

[c]For any cube set for any route, if the matching cube set was absent the PBS value used was the global mean determined as the mean of all averaged PBS cube sets and has a value of 28.1 nmol/mg·hr.

[d]The percentage of cubes positive for each category was calculated on the basis of total cubes for each monkey, which varied between 77 and 97 of cubes per brain.

Another way to analyze the cube data in Fig. 3 was to compare the number of cubes with positive increases in ARSA expression for the five surgical routes of delivery, with the data plotted by percentage of total brain cubes grouped by treatment (Fig. 4A). The data were plotted as the number of 1-cm^3 brain cubes that had an increase in ARSA activity greater than 10, 25, or 50% relative to the PBS control/wild-type mean levels ($n=2$ per route, except for the intraarterial route). As summarized in Table 2 for the three best routes of administration, the percentage of positive cubes >10% relative to mean wild-type levels from PBS controls ranged between 58 and 80, the percentage of positive cubes >25% ranged between 36 and 61, and the percentage of positive cubes >50% ranged between 21 and 32, with the white matter delivery route being the best in all three categories.

Additional analysis of ARSA enzymatic assay data from the 1-cm^3 cubes was performed to assess the delivery route that provided the widest distribution across the CNS. To determine the widest distribution, the individual brain cube data per coronal slice was compiled for each NHP, and used to determine the mean percent increase relative to the PBS background for each slice. The means were plotted versus the coronal slice location, rostral to caudal, for each of the five routes of administration (Fig. 4B–E). On the basis of the sectioning of the brains during necropsy, the white matter route infusions were into coronal slices S3–S5, and the deep gray matter with overlying white matter route infusions (caudate, putamen, and thalamus) were into coronal slices S2–S4 (Supplementary Fig. S1). The relative locations of brain substructures in coronal slices were as follows: caudate nucleus (S2–S5), putamen (S3–S4), thalamus (S4–S5), hippocampus (S4–S5), and cerebellum (S5–S7). The peak activity for both the white matter and deep gray matter with overlying white matter routes was in coronal slice S4, and that for deep gray matter with convection-enhanced delivery was in slice S2 (Fig. 4B–D). Whereas, the white matter route displays percent increase in ARSA at consistent levels >40% across the brain sections, the deep gray matter routes appear to be more localized to the regions of administration. Not surprisingly, based on the individual cube data, the intraventricular and intraarterial routes failed to display any ''positive'' coronal slices (Fig. 4E). The results of this analysis support the conclusion that the white matter delivery route yielded the widest distribution.

ARSA expression in the spinal cord

As MLD also impacts the distal and peripheral nervous system, samples were taken from various levels of the spinal cord, assessed for levels of ARSA resulting from each route of administration, and compared with the PBS control by enzymatic activity assay. The same cord sections (cervical C3, thoracic T4, lumbar L4) were excised for each nonhuman primate, analyzed for ARSA activity, averaged for each route ($n=2$), and expressed as the percent increase relative to PBS background for each spinal cord section.

There was only a modest increase in ARSA levels relative to the controls for both the cervical and thoracic spinal samples, but a more significant increase was observed in the lumbar spinal samples for all routes, except for the intraarterial route (data not shown). The white matter, deep gray matter with overlying white matter, and deep gray matter using convection-enhanced delivery routes all demonstrated more than a 40% increase in ARSA activity and greater than 2 standard deviations over background levels for lumbar spinal samples. The intraventricular and intraarterial routes failed to show a similar increase in spinal

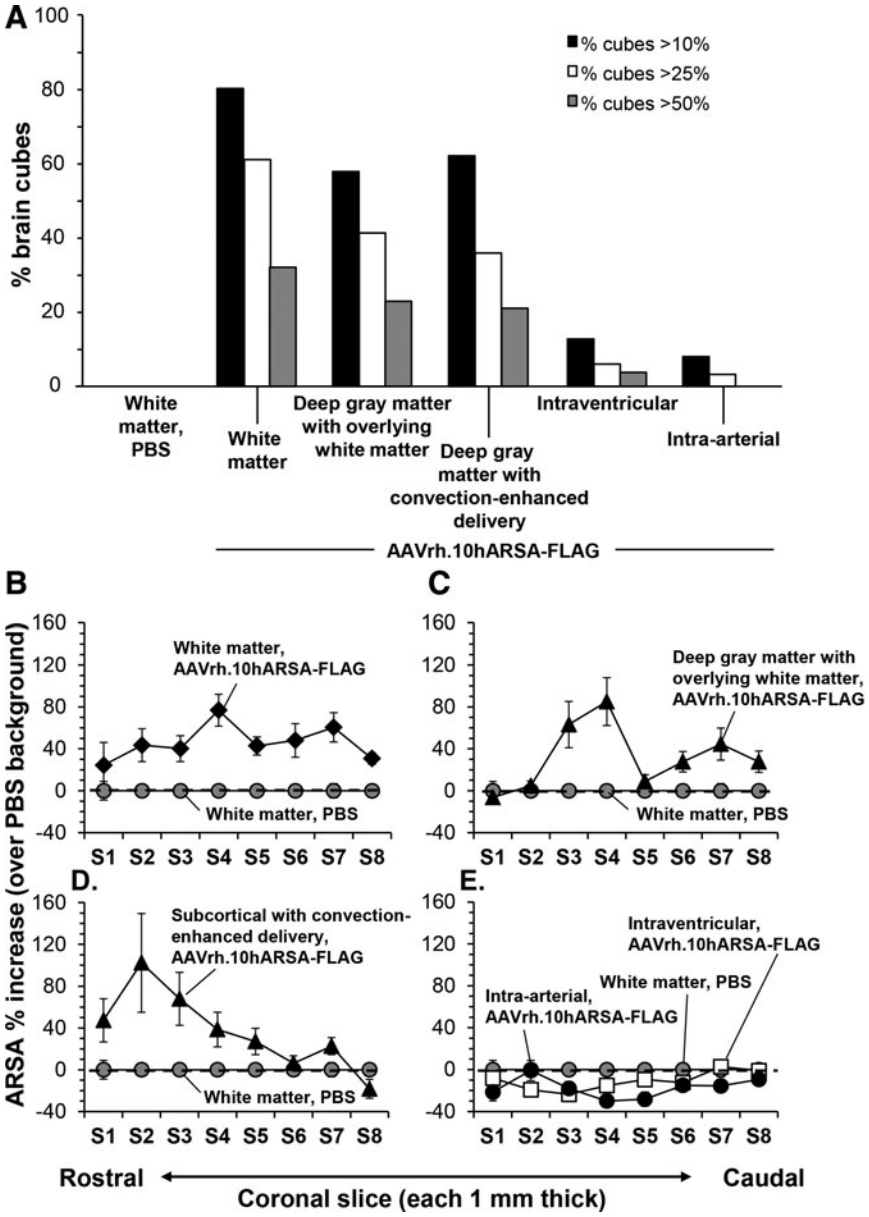

FIG. 4. Comparison of increased ARSA activity in the CNS after AAVrh.10hARSA-FLAG administration via five surgical routes in nonhuman primates. As described in Fig. 3, the right hemispheres of nonhuman primate brains were subdivided into 1-cm^3 cubes and analyzed for ARSA enzymatic activity. ARSA values were corrected using paired-matched brain cube sets of PBS control nonhuman primates, and then expressed as the percent increase above the PBS (wild-type monkey) background mean corresponding to that cube set. **(A)** Comparison of the percentage of 1-cm^3 brain cubes displaying increased ARSA activity relative to endogenous background (PBS controls) at >10, >25, and >50% levels. The percentage of cubes positive for each category was calculated on the basis of total cubes for each monkey, which varied between 77 and 97 cubes per brain. The route of vector administration is displayed along the abscissa for each group of three columns. The percentage of total brain cubes displaying an increase >10% (black columns), >25% (white columns), and >50% (gray columns) is shown for each treatment. **(B–E)** Comparison of ARSA activity in each coronal section for each surgical route. The mean ARSA percent increase was determined for each coronal slice by averaging the percent increase for all cubes in that section. Means are shown with SEM. Negative values indicate a value less than the PBS mean for that specific cube set. The dashed line represents the mean PBS background (0%). Coronal slices (width, 1 mm^2) are displayed from the anterior to the posterior end of the NHP brains. The controls received PBS in place of AAVrh.10hARSA-FLAG via white matter administration. The surgical routes are compared with the PBS controls (baseline): **(B)** white matter, **(C)** deep gray matter with overlying white matter, **(D)** deep gray matter using convection-enhanced delivery, and **(E)** intraventricular and intraarterial. Deep gray matter routes infused into the caudate, putamen, and thalamus, whereas the white matter routes targeted the centrum semiovale white matter. Relative locations of brain substructures in coronal slices: caudate nucleus (S3–S5), putamen (S3–S4), thalamus (S4–S5), hippocampus (S4–S5), cerebellum (S5–S7).

cord ARSA levels, mediating a modest 15% increase for the intraventricular route of delivery. However, immunohistochemistry of the spinal cord and dorsal root ganglia from one monkey receiving intraventricular vector displayed positive staining for ARSA-FLAG at all three levels of the spinal cord, including the lumbar L4 dorsal white matter tracts, dorsal nerve roots, gray matter dorsal and ventral horns, and dorsal root ganglia (Supplementary Fig. S3). Positive detection of ARSA-FLAG in the lumbar dorsal root ganglion samples by immunohistochemistry was also observed in one of two monkeys for the deep gray matter with overlying white matter and deep gray matter with convection-enhanced delivery routes of administration; in contrast, no FLAG was detected in the lumbar dorsal root ganglion samples for the white matter and intraarterial routes. This finding indicates that the intraventricular surgery was successful at least in placing vector into the lumbar spinal region, and suggests that the vector may have followed the spinal fluid flow toward the spinal cord rather than into the brain parenchyma.

Neutralizing antibodies

Because the presence of high levels of systemic anti-AAV immunity may dampen AAVrh.10hARSA-FLAG-mediated expression of ARSA, we monitored the monkeys for development of neutralizing anti-AAV antibodies in the serum before and after vector administration (Fig. 5). All nonhuman primates in this trial had undetectable serum anti-AAVrh.10 neutralizing antibody titers before vector administration. After vector administration, only one monkey (intraventricular route) evoked neutralizing titers above the 1:100 level (on day 7). This increase was transient and decreased to the 1:10 level by the end of the study. Several nonhuman primates had modest increases in anti-AAVrh.10 neutralizing titers during the course of the experiment, and of these, only two displayed a minor elevation of titer (1:20) by the end of trial. At the end of the study 8 of the 11 monkeys had no detectable anti-AAVrh.10 neutralizing antibodies (Fig. 5). This is consistent with our previous study in support of the LINCL clinical trial, in which we administered AAVrh.10 to the CNS of nonhuman primates (Hackett *et al.*, 2005).

Postsurgical assessment

In addition to the comparative measures of efficacy of distribution between the routes of administration, the go/no go criteria for clinical development require safety and toxicological evaluation. We therefore evaluated the impact of CNS administration of AAVrh.10hARSA-FLAG via the various routes on the behavior of nonhuman primates. All nonhuman primates were monitored in videotaped sessions three times before surgery and 7, 14, 28, 56, and 91 days after vector administration for behavioral assessment with and without the stimulus of food and threat scenario. Each animal was videotaped for 3 min and analyzed by observers ($n=2$) blinded to the treatment group and time of assessment for 20 different primate behaviors (shown in Supplementary Table S1; normal, $n=14$ and abnormal, $n=6$), scoring ''1'' for 5 sec of each behavior. The sum of normal typical primate behavior scores (''healthy score sum'') was averaged for each treatment ($n=2$) and plotted at eight time points (five of them postsurgery) (Fig. 6). The healthy score sum normal reference range (scores, 3.5 to 50.2) was determined as the mean of presurgery scores ± 2 standard deviations. No difference was seen between the PBS- versus AAV-treated nonhuman primates for any route of administration [two-way RM-ANOVA, $p>0.37$, $F(35,35)=1.11$]. There were no observations of abnormal behavior such as sedation or neurological deficits and tics at any point during the 3-month study for any route of vector or PBS administration. In all cases, animals responded appropriately and without hesitation or delayed movement and at no point were tremors, seizures, or other abnormal neuropathies observed. Only a few episodes of transient stereotypy behavior (e.g., prolonged scratching) were observed. None of the nonhuman primates had any delayed response to food or specific threatening scenarios. In summary, behavior analysis demonstrated no adverse effects for any surgical route of vector administration.

In addition to behavior, the nonhuman primates were assessed twice presurgery, on day 0 (day of surgery), and on days 2, 7, 14, 28, 56, and 91 (day of sacrifice) for general health and safety parameters by serum chemistry (Supplementary Fig. S4)

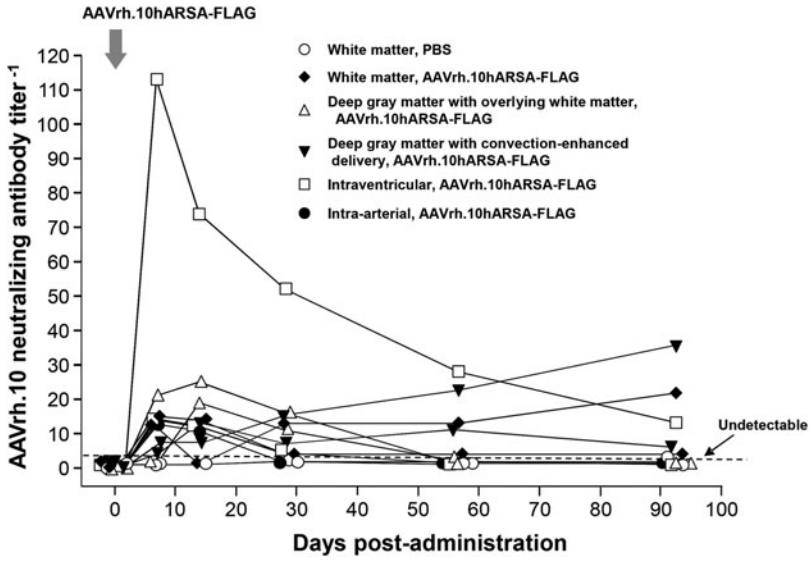

FIG. 5. Assessment in nonhuman primates of neutralizing anti-AAV antibody titers evoked by administration of AAVrh.10hARSA-FLAG. Nonhuman primates ($n=11$) were administered AAVrh.10hARSA-FLAG (1.5×10^{12} GC) as described in Table 1. Neutralizing antibody titers were determined over time. The neutralizing antibody titer is expressed as the reciprocal of the serum dilution at which 50% inhibition of AAVrh.10Luc was observed. Titers were evaluated presurgery, on day 0 (the day of surgery), and postsurgery on days 2, 7, 14, 28 and 56, and 91 (at necropsy).

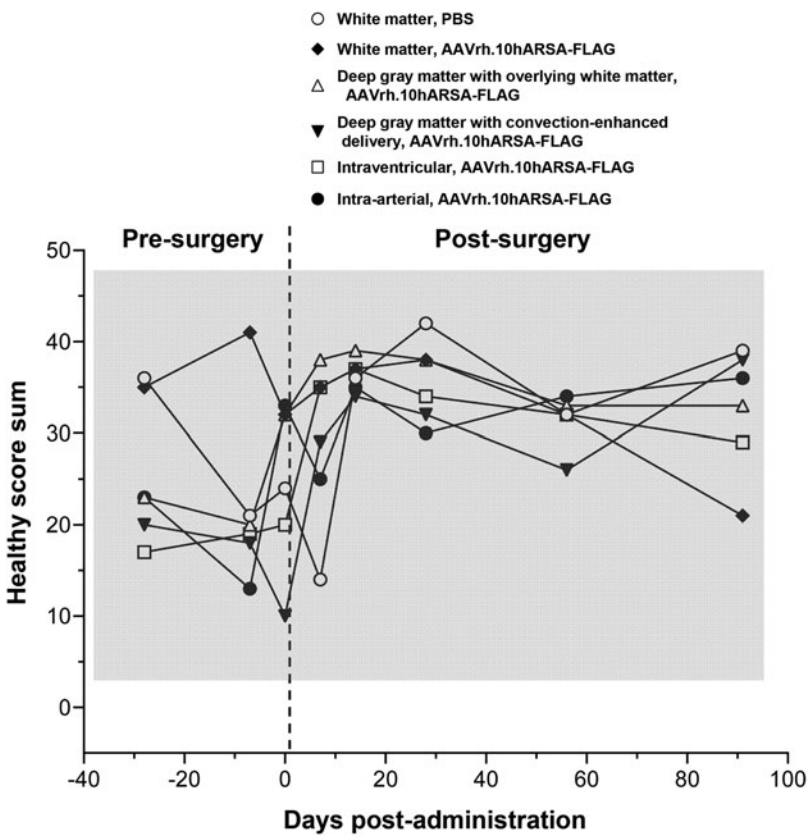

FIG. 6. Assessment of nonhuman primate behavior for changes in healthy behavior attributable to surgical route or vector administration. African green monkeys administered AAVrh.10hARSA-FLAG (1.5×10^{12} GC) or PBS were assessed for behavioral activity over the 13-week trial. The nonhuman primates were videotaped for activity, abnormal activity, or lack of any activity, at presurgery (days -28 and -7), the day of surgery (day 0), and days 7, 14, 28, 56, and 91 postsurgery. Each animal was videotaped for 3 min in the absence of outside stimuli and subsequently analyzed by 2 blinded observers for 20 specific primate behaviors (normal, $n=14$ and abnormal, $n=6$), scoring ''1'' for 5 sec of each behavior. The sum of normal typical primate behaviors (anxiety, arousal, and quiet groups) was calculated as a ''healthy'' score (defined in Supplementary Table S1) for each session and plotted as the mean of each treatment group ($n=2$, except for intraarterial where $n=1$) as a function of time. The shaded area represents normal (presurgical) values ± 2 standard deviations. No difference was seen between the PBS versus AAV-treated NHPs [two-way repeated-measures ANOVA, $p>0.37$, $F(35,35)=1.11$].

and hematology by complete blood count analysis (Supplementary Fig. S5). Values for each of the parameters were plotted for individual animals, with the upper and lower limits of normal African green monkey ranges (Liddie *et al.*, 2010). The analyses were performed in a blinded fashion. There were no adverse trends in these parameters for any of the five surgical routes; only day 2 postsurgery comparisons showed significance when all the animals were compared together (Supplementary Table S2). Statistical analyses between the PBS controls and each group of animals receiving surgical administration revealed only a few parameters with a significant difference (e.g., PBS vs. deep gray matter with overlying white matter route [alkaline phosphatase, aspartate aminotransferase, creatine kinase]; Supplementary Table S3), and these may be due to the surgery and anesthesia. Except for transient increases in a few liver/muscle enzymes (alanine aminotransferase, aspartate aminotransferase, lactate dehydrogenase, creatine kinase), none of the treated nonhuman primates had abnormal serum chemistries postsurgery and, importantly, all transient serum parameter elevations were resolved by day 14. No complications from any of vector delivery routes were noted. There were no acute rapid elevations noted in the hematologic parameters. The white blood counts varied, but were within normal parameters. There was a transient decrease in lymphocytes and corresponding increase in monocytes during week 1 postsurgery, but all changes were quickly resolved.

Discussion

There are currently no approved therapies for metachromatic leukodystrophy (Batzios and Zafeiriou, 2012; Patil and Maegawa, 2013). Similar to other lysosomal storage disorders, the genetic defect in MLD affects the ability of the cells to maintain lysosomal homeostasis, causing a buildup of toxic by-products in the lysosomes that in turn leads to apoptosis (Patil and Maegawa, 2013). Because manifestations of the disease can affect the cells of the brain, spinal cord, and peripheral nerves, the main roadblock to therapy has been to achieve and maintain therapeutic levels of the ARSA enzyme in the CNS and PNS (Krivit *et al.*, 1999; Gray, 2013). As the pathological effects of the lysosomal storage disorder are most dramatic in the CNS, any therapies for MLD must target the most affected organ, the brain, and stem the neuronal loss and devastating resulting pathology. Hence, in order for gene therapy to become a reality for MLD, any treatment must provide widespread ARSA at therapeutic levels across much of the brain. In this study we evaluated several routes of administration to safely deliver normal copies of the ARSA gene to cells of the CNS, and to persistently express ARSA.

Approaches to therapy of MLD

Various therapeutic approaches to correcting or stabilizing MLD have been tested to date, including enzyme replacement therapy, bone marrow transplantation, transplantation of stem cells modified via *ex vivo* gene therapy, and direct administration of viral vectors expressing ARSA to the brain (Batzios and Zafeiriou, 2012; Patil and Maegawa, 2013). Enzyme replacement therapies (ERTs) have been successful in preventing or reversing the systemic manifestations of several lysosomal storage disorders by taking advantage of transcytosis of infused soluble enzymes to lysosomes via the M6P receptors, which are present on the surface of most cells

(Funk *et al.*, 1992; Ghosh *et al.*, 2003). Intravenous administration of recombinant ARSA in the MLD mouse model reduced sulfatide storage in the brain and peripheral nerves, but was efficacious only when injected into young mice (Matzner *et al.*, 2005; Matthes *et al.*, 2012). This therapeutic approach has promise for prevention or reversal of demyelination in the peripheral nerves of patients with MLD, but the extent of metabolic correction is unlikely to be sufficient and timely in arresting the rapid cerebral demyelinating process that occurs in the aggressive and devastating forms of infantile and early juvenile forms of MLD. Several clinical trials have been established to study ERT in patients with MLD; however, none have yet shown efficacy. One trial, the IDEAMLD phase 1/2 clinical trial for ERT in MLD (NCT01510028; http://clinicaltrials.gov/), is ongoing with no preliminary results posted. To circumvent the blood–brain barrier issue, the patients are being treated with recombinant ARSA (HGT-1110; Shire Human Genetic Therapies, Cambridge, MA), administered every other week via an intrathecal drug delivery device for 38 weeks.

One therapeutic modality that has shown some success is the use of hematopoietic cell transplantation in presymptomatic children with MLD (Bayever *et al.*, 1985; Krivit *et al.*, 1999). This beneficial effect is likely mediated by bone marrow-derived stem cells that migrate into the brain and differentiate into microglia that produce normal copies of the ARSA enzyme (Asheuer *et al.*, 2004; Biffi *et al.*, 2006). When performed at an early stage of the disease, hematopoietic cell transplantation can stabilize the cerebral demyelination in patients with late-onset MLD (juvenile and adult forms) (Krivit *et al.*, 1999; Sevin *et al.*, 2007). However, in the more severe infantile and early juvenile form of MLD, hematopoietic cell transplantation does not arrest the rapid progression of cerebral demyelination, even when the procedure is performed early in presymptomatic infants (Bredius *et al.*, 2007). Given the slow pace of brain microglia replacement by bone marrow-derived cells, hematopoietic stem cell gene therapy may not be able to prevent the rapid cerebral demyelination that occurs in early and late infantile forms of MLD (Krivit *et al.*, 1995; Kennedy and Abkowitz, 1997; Chan *et al.*, 2007). Results from a clinical trial in patients with late infantile MLD, using allogeneic, autologous lentivirus-mediated genetically modified hematopoietic stem cells expressing ARSA, suggest that the disease progression can be halted if treatment is administered early to presymptomatic patients (Biffi *et al.*, 2013). It remains to be evaluated in symptomatic children manifesting rapidly declining forms of MLD (Matthes *et al.*, 2012). Unfortunately, until genetic screening for MLD is included in the battery of neonatal tests, the vast majority of patients afflicted with MLD will not be diagnosed in the presymptomatic phase (Matthes *et al.*, 2012).

For direct CNS gene therapy, AAV vectors have emerged as the most promising clinical vector because of their excellent safety and efficacy profile (Sevin *et al.*, 2007; Sondhi *et al.*, 2008). AAV-based therapies to the CNS have been assessed in Canavan, late infantile neuronal ceroid lipofuscinosis (LINCL), Alzheimer's, and Parkinson's diseases (Janson *et al.*, 2002; Tuszynski and Blesch, 2004; McPhee *et al.*, 2006; Kaplitt *et al.*, 2007; Worgall *et al.*, 2008; Mandel, 2010; Souweidane *et al.*, 2010; Kells *et al.*, 2012). Direct gene therapy producing a secreted protein gene product to the CNS leverages cross-correction of noninfected neighboring cells, irrespective of cell type, thereby increasing the extent of defect correction and thus enhancing the potential for success of the therapy.

Although it has been shown that AAV serotypes such as AAV9 can cross the blood–brain barrier and transduce brain parenchyma in rodents and nonhuman primates (Gray, 2013; Samaranch *et al.*, 2014), intravenous applications are relatively inefficient, with most of the vector remaining in the viscera and unlikely to be efficacious for diffuse CNS disorders such as MLD. At the high vector dose necessary to achieve brain expression in adult mice ($>1.5\times10^{12}$ genome copies [GC]/kg) (Maguire *et al.*, 2013), translation to human application will require massive levels of vector, with possible adverse effects. The biggest challenges for success of an intravenous route of AAV infusion are as follows: (1) the dosage necessary to treat the CNS will likely be $>10^{14}$ GC/kg; and (2) the immunogenicity to that large AAV dose is potentially a safety concern (Mingozzi and High, 2013). These doses are 1–2 logs higher than that being tested in current human AAV gene therapy trials, and thus unlikely to be reasonable for translation to human use (High, 2012). As an alternative, the minimally invasive administration to cerebral spinal fluid via the cisterna magna reservoir in nonhuman primates has shown that intracisternal infusion of AAV vectors (i.e., AAV7 and AAV9) results in widespread cortical neuronal expression of transgenes (Gray, 2013; Bankiewicz, 2014; Samaranch *et al.*, 2014). Because of limitations typical for nonhuman primate studies, we chose not to investigate the use of several AAV serotypes via multiple routes of administration, instead focusing on the one serotype, AAVrh.10.

AAV vector direct CNS therapy of MLD

The AAVrh.10 vector is the leading candidate to treat the CNS manifestations of MLD. Preclinical efficacy data in ARSA-deficient mice (MLD mice) demonstrated that the use of AAV5 and AAVrh.10 vectors provides high levels of transgene expression, spread of the human ARSA enzyme throughout the brain, with concomitant improvement of the neurologic phenotype (Sevin *et al.*, 2006, 2007). Assessment of MLD mice also indicated that the delivery system for the same genetic payload with the capsid of AAVrh.10 provides higher levels and better spread of the therapeutic protein than AAV5 (Piguet *et al.*, 2012). ARSA produced by neurons in AAVrh.10-treated MLD mice can be secreted and taken up at a distance by other CNS cells including oligodendrocytes. In addition, because the AAVrh.10 vector is derived from rhesus macaques, preexisting anti-AAV vector humoral immunity is unlikely to be a significant barrier to gene transfer to humans (De *et al.*, 2006; Sondhi *et al.*, 2007; Zaiss *et al.*, 2008).

The present nonhuman primate study was designed to determine whether AAVrh.10 vector encoding the normal human ARSA cDNA is capable of delivering therapeutic levels of ARSA enzyme to the CNS of nonhuman primates and which route is best to obtain the maximal distribution of transgene product across the CNS. We compared the current human vector administration protocol (direct white matter) for the LINCL clinical study (Worgall *et al.*, 2008; Souweidane *et al.*, 2010) with four alternative protocols focusing on ARSA

distribution criteria. The total dose administered in this study (1.5×10^{12} GC) was based on the projected therapeutic levels for clinical trials and used in our prior study with AAV5-hARSA (Colle *et al.*, 2010). In our LINCL trial we administered vector exclusively to the white matter underlying the cortex, using small-bore catheters directed to predetermined locations with guide needles, with two injection levels through each of six symmetrically located burr holes. We compared delivery to the white matter with delivery to alternative locations chosen on the basis of well-described connected afferent and efferent neuronal pathways (Gould, 2013), and assessed the impact of gradually ramping up the infusion speed by convection-enhanced delivery to these alternative locations (Krauze *et al.*, 2005; Sebastian *et al.*, 2012). In addition to direct cerebral delivery, we assessed intraventricular delivery of AAV, a method commonly used for drug delivery, and a nonsurgical route, in which the cerebral vasculature is used to deliver the vector via the intraarterial route with mannitol to assist in translocating the vector across the blood–brain barrier.

Direct administration of AAVrh.10hARSA-FLAG to the brain parenchyma (white matter, deep gray matter with overlying white matter, and deep gray matter with convection-enhanced delivery) generated significantly elevated levels of ARSA enzymatic activity above the therapeutic threshold (5–10%) throughout the brains of nonhuman primates. Immunohistochemistry of treated nonhuman primates confirmed these results, with detection of extensive multifocal ARSA deposits resulting from the three intraparenchymal routes of delivery in the cortex, white matter, deep gray matter of the striatum, thalamus, choroid plexus, and spinal cord dorsal root ganglia. In contrast, the intraventricular and intraarterial routes of delivery of vector failed to demonstrate measurable levels of ARSA activity relative to sham PBS-treated controls and showed a similar lack of immunohistochemical detection in the CNS. ARSA activity was observed in the spinal cord for all three intraparenchymal and intraventricular routes, with the lumbar region displaying the highest levels. We cannot conclude whether the ARSA activity concentrated in the lumbar samples was due to antegrade translocation of AAVrh.10 vector or to simple diffusion of the enzyme.

While the intraarterial route with mannitol pretreatment failed to demonstrate any ARSA activity greater than the endogenous control background, it is possible that this failure was due to the limited exposure time to mannitol that was employed before vector administration. Other studies have explored longer mannitol pretreatment exposure times, up to 10 min, before therapeutic delivery of drugs in rodents (McCarty 2009, Bevan 2014).

As MLD affects the white matter, it was encouraging to observe that intraparenchymal administration of AAVrh .10hARSA-FLAG led to positive detection of ARSA-FLAG deposits in glial cells, based on their morphology, and in axon bodies in the white matter, proximal and distal to the sites of vector administration, when using the white matter and deep gray matter with overlying white matter routes of delivery. Because the vector was administered in multiple loci in this study, it was not possible to determine whether the enzyme spread was due to retrograde axonal transport of the vector or to uptake through the M6P receptor system, or occurred by an unknown mechanism (Funk *et al.*, 1992; Ghosh *et al.*, 2003; Kells *et al.*, 2012). Because this was not a formal safety and toxicology study, determination of the biodistribution of the AAVrh.10 vector in the brain and visceral organs was not performed in this study; instead we focused on the efficacy-related distribution of the transgene end-product, ARSA enzyme, to specify potential therapeutic coverage across the brain as a comparison for the various routes of administration. The data demonstrate that AAVrh.10-mediated delivery of the ARSA transgene via the white matter route in the nonhuman primate CNS resulted in the broadest distribution of ARSA, with dramatically increased ARSA enzymatic activity well above therapeutic minimums. Given the established persistence of expression of AAV vectors, this suggests that similar enzymatic levels could provide life-long therapeutic benefits for patients with MLD.

Mild histiocytic infiltrates and linear glial scars along the needle tracks are expected from the mechanical disruption of the catheter, and this was confirmed by the presence of these lesions in PBS-treated animals. However, we also observed areas of white and gray matter lymphohistiocytic infiltrates, often but not always in combination with white matter degeneration and loss accompanied by gliosis, in all animals that received AAVrh.10hARSA-FLAG by intracerebral injection. Because these changes were localized at each injection sites, were strongly associated with FLAG staining by immunohistochemistry, and were not observed in PBS-treated animals, a causative involvement of AAVrh.10hARSA-FLAG in the development of those lesions is probable. However, the mechanism by which AAVrh.10hARSA-FLAG may have caused these lesions is unclear. No clinical abnormalities correlated with these findings. However, our study was not a formal toxicology study. The FLAG-tagged ARSA protein is a tool for evaluating breadth of expression with potential immunological implications irrelevant to the candidate therapeutic. Foreign proteins such as green fluorescent protein have been shown to generate immune-mediated brain lesions in nonhuman primates similar to our findings, even if delivered by the noninvasive intracisternal route (Samaranch *et al.*, 2014). Therefore, an immune reaction to the FLAG peptide appears to be a possible explanation for the lesions we observed. An ongoing formal toxicology study aims to evaluate whether these untoward effects are observed with the AAVrh.10-vectored human ARSA transgene without FLAG, the candidate therapeutic.

The data also demonstrated that AAVrh.10 vector administration directly to the brain had minimal side effects. No overt neurological behavioral changes were observed during postsurgical surveillance throughout the 13-week study. Insignificant increases were noted for anti-AAV neutralizing antibody serum titers, suggesting that readministration of the same vector might be feasible and efficacious. Analysis of the blood cell count and serum chemistries from AAVrh.10-hARSA-FLAG-treated nonhuman primates in comparison with PBS-sham controls showed no vector-related significance. Postsurgical elevations in liver and muscle enzyme levels, typically seen after surgery with anesthesia, were quickly resolved by day 14. No complications from the surgeries were observed in nonhuman primate health or behavior, demonstrating that the vector and surgery were well tolerated. Also, minimal anti-AAVrh.10 antibodies were

detected, suggesting that readministration of the same vector might be feasible and efficacious.

In summary, the present study demonstrates that AAVrh.10 vectors can deliver ARSA to a large proportion of the CNS of a large animal on a persistent basis. We have found that the deep gray matter with overlying white matter route generated focal high expression of ARSA, but it was only with the white matter route that dispersed widespread expression was observed across the length and breadth of the CNS. An ongoing formal safety and toxicology study will evaluate immunohistochemical findings with respect to the FLAG tag. This, combined with the lack of safety issues related to behavior, hematology, and serum chemistry parameters for treated monkeys and our clinical trial experience with this vector for LINCL, will allow us to determine whether this route of delivery will be well tolerated.

Acknowledgments

The authors thank Victor Brodsky and Liza Rivera of the New York Presbyterian Pathology Department for assistance with the slide scans; Rodolfo Ricart-Arbona for veterinary help; and N. Mohamed for help in preparing this manuscript. These studies were supported, in part, by U01NS066920.

Author Disclosure Statement

No competing financial interests exist.

References

Asheuer, M., Pflumio, F., Benhamida, S., *et al*. (2004). Human $CD34^+$ cells differentiate into microglia and express recombinant therapeutic protein. Proc. Natl. Acad. Sci. U.S.A. 101, 3557–3562.

Aubourg, P., Sevin, C., and Cartier, N. (2011). Mouse models of metachromatic leukodystrophy and adrenoleukodystrophy. In *Animal Models of Dementia*. P.P. De Deyn and D. Van Dam, eds. (Springer Science + Business Media, Philadelphia, PA), *pp.* 493–513.

Bankiewicz, K. (2014). Neurosurgical approaches: Drug infusion directly into the parenchyma or the cerebrospinal fluid. In *Drug Delivery to the Brain*. M. Hammarlund-Udenaes, E.C.M. de Lange, and R.G. Thorne, eds. (Springer, New York), *pp.* 501–518.

Batzios, S.P., and Zafeiriou, D.I. (2012). Developing treatment options for metachromatic leukodystrophy. Mol. Genet. Metab. 105, 56–63.

Bayever, E., Ladisch, S., Philippart, M., *et al*. (1985). Bone-marrow transplantation for metachromatic leucodystrophy. Lancet 2, 471–473.

Beck, M. (2007). New therapeutic options for lysosomal storage disorders: Enzyme replacement, small molecules and gene therapy. Hum. Genet. 121, 1–22.

Biffi, A., De, P.M., Quattrini, A., *et al*. (2004). Correction of metachromatic leukodystrophy in the mouse model by transplantation of genetically modified hematopoietic stem cells. J. Clin. Invest. 113, 1118–1129.

Biffi, A., Capotondo, A., Fasano, S., *et al*. (2006). Gene therapy of metachromatic leukodystrophy reverses neurological damage and deficits in mice. J. Clin. Invest. 116, 3070–3082.

Biffi, A., Montini, E., Lorioli, L., *et al*. (2013). Lentiviral hematopoietic stem cell gene therapy benefits metachromatic leukodystrophy. Science 341, 1233158.

Bredius, R.G., Laan, L.A., Lankester, A.C., *et al*. (2007). Early marrow transplantation in a pre-symptomatic neonate with late infantile metachromatic leukodystrophy does not halt disease progression. Bone Marrow Transplant. 39, 309–310.

Chan, W.Y., Kohsaka, S., and Rezaie, P. (2007). The origin and cell lineage of microglia: New concepts. Brain Res. Rev. 53, 344–354.

Colle, M.A., Piguet, F., Bertrand, L., *et al*. (2010). Efficient intracerebral delivery of AAV5 vector encoding human ARSA in non-human primate. Hum. Mol. Genet. 19, 147–158.

De, B.P., Heguy, A., Hackett, N.R., *et al*. (2006). High levels of persistent expression of α_1-antitrypsin mediated by the non-human primate serotype rh.10 adeno-associated virus despite preexisting immunity to common human adeno-associated viruses. Mol. Ther. 13, 67–76.

Funk, B., Kessler, U., Eisenmenger, W., *et al*. (1992). Expression of the insulin-like growth factor-II/mannose-6-phosphate receptor in multiple human tissues during fetal life and early infancy. J. Clin. Endocrinol. Metab. 75, 424–431.

Ghosh, P., Dahms, N.M., and Kornfeld, S. (2003). Mannose 6-phosphate receptors: New twists in the tale. Nat. Rev. Mol. Cell. Biol. 4, 202–212.

Gieselmann, V., and Krageloh-Mann, I. (2010). Metachromatic leukodystrophy—an update. Neuropediatrics 41, 1–6.

Gieselmann, V., Franken, S., Klein, D., *et al*. (2003). Metachromatic leukodystrophy: Consequences of sulphatide accumulation. Acta Paediatr. Suppl. 92, 74–79.

Gould, D.J. (2013). *Lippincott's Pocket Neuroanatomy*. (Lippincott Williams & Wilkins, Philadelphia, PA).

Gray, S.J. (2013). Gene therapy and neurodevelopmental disorders. Neuropharmacology 68, 136–142.

Hackett, N.R., Redmond, D.E., Sondhi, D., *et al*. (2005). Safety of direct administration of $AAV2_{CU}$hCLN2, a candidate treatment for the central nervous system manifestations of late infantile neuronal ceroid lipofuscinosis, to the brain of rats and nonhuman primates. Hum. Gene Ther. 16, 1484–1503.

High, K.A. (2012). The gene therapy journey for hemophilia: Are we there yet? Blood 120, 4482–4487.

Janson, C., McPhee, S., Bilaniuk, L., *et al*. (2002). Clinical protocol: Gene therapy of Canavan disease: AAV-2 vector for neurosurgical delivery of aspartoacylase gene (ASPA) to the human brain. Hum. Gene Ther. 13, 1391–1412.

Kaplitt, M.G., Feigin, A., Tang, C., *et al*. (2007). Safety and tolerability of gene therapy with an adeno-associated virus (AAV) borne GAD gene for Parkinson's disease: An open label, phase I trial. Lancet 369, 2097–2105.

Kells, A.P., Forsayeth, J., and Bankiewicz, K.S. (2012). Glial-derived neurotrophic factor gene transfer for Parkinson's disease: Anterograde distribution of AAV2 vectors in the primate brain. Neurobiol. Dis. 48, 228–235.

Kennedy, D.W., and Abkowitz, J.L. (1997). Kinetics of central nervous system microglial and macrophage engraftment: Analysis using a transgenic bone marrow transplantation model. Blood 90, 986–993.

Krauze, M.T., Saito, R., Noble, C., *et al*. (2005). Reflux-free cannula for convection-enhanced high-speed delivery of therapeutic agents. J. Neurosurg. 103, 923–929.

Krivit, W., Sung, J.H., Shapiro, E.G., *et al.* (1995). Microglia: The effector cell for reconstitution of the central nervous system following bone marrow transplantation for lysosomal and peroxisomal storage diseases. Cell Transplant. 4, 385–392.

Krivit, W., Aubourg, P., Shapiro, E., *et al*. (1999). Bone marrow transplantation for globoid cell leukodystrophy, adrenoleukodystrophy, metachromatic leukodystrophy, and Hurler syndrome. Curr. Opin. Hematol. 6, 377–382.

Liddie, S., Goody, R.J., Valles, R., *et al*. (2010). Clinical chemistry and hematology values in a Caribbean population of African green monkeys. J. Med. Primatol. 39, 389–398.

Maguire, C.A., Crommentuijn, M.H., Mu, D., *et al*. (2013). Mouse gender influences brain transduction by intravascularly administered AAV9. Mol. Ther. 21, 1470–1471.

Mandel, R.J. (2010). CERE-110, an adeno-associated virus-based gene delivery vector expressing human nerve growth factor for the treatment of Alzheimer's disease. Curr. Opin. Mol. Ther. 12, 240–247.

Matthes, F., Stroobants, S., Gerlach, D., *et al*. (2012). Efficacy of enzyme replacement therapy in an aggravated mouse model of metachromatic leukodystrophy declines with age. Hum. Mol. Genet. 21, 2599–2609.

Matzner, U., Harzer, K., Learish, R.D., *et al*. (2000). Long-term expression and transfer of arylsulfatase A into brain of arylsulfatase A-deficient mice transplanted with bone marrow expressing the arylsulfatase A cDNA from a retroviral vector. Gene Ther. 7, 1250–1257.

Matzner, U., Herbst, E., Hedayati, K.K., *et al*. (2005). Enzyme replacement improves nervous system pathology and function in a mouse model for metachromatic leukodystrophy. Hum. Mol. Genet. 14, 1139–1152.

McPhee, S.W., Janson, C.G., Li, C., *et al*. (2006). Immune responses to AAV in a phase I study for Canavan disease. J. Gene Med. 8, 577–588.

Mingozzi, F., and High, K.A. (2013). Immune responses to AAV vectors: Overcoming barriers to successful gene therapy. Blood 122, 23–36.

Miranda, C.O., Brites, P., Mendes, S.M., *et al*. (2013). Advances and pitfalls of cell therapy in metabolic leukodystrophies. Cell Transplant. 22, 189–204.

Molander-Melin, M., Pernber, Z., Franken, S., *et al*. (2004). Accumulation of sulfatide in neuronal and glial cells of arylsulfatase A deficient mice. J. Neurocytol. 33, 417–427.

Patil, S.A., and Maegawa, G.H. (2013). Developing therapeutic approaches for metachromatic leukodystrophy. Drug Des. Devel. Ther. 7, 729–745.

Piguet, F., Sondhi, D., Piraud, M., *et al*. (2012). Correction of brain oligodendrocytes by AAVrh.10 intracerebral gene therapy in metachromatic leukodystrophy mice. Hum. Gene Ther. 23, 903–914.

Rauschka, H., Colsch, B., Baumann, N., *et al*. (2006). Late-onset metachromatic leukodystrophy: Genotype strongly influences phenotype. Neurology 67, 859–863.

Samaranch, L., San, S.W., Kells, A.P., *et al*. (2014). AAV9-mediated expression of a non-self protein in nonhuman primate central nervous system triggers widespread neuroinflammation driven by antigen-presenting cell transduction. Mol. Ther. 22, 329–337.

Sebastian, W.S., Richardson, R.M., Kells, A.P., *et al*. (2012). Safety and tolerability of magnetic resonance imaging-guided convection-enhanced delivery of AAV2-hAADC with a novel delivery platform in nonhuman primate striatum. Hum. Gene Ther. 23, 210–217.

Sevin, C., Benraiss, A., Van, D.D., *et al*. (2006). Intracerebral adeno-associated virus-mediated gene transfer in rapidly progressive forms of metachromatic leukodystrophy. Hum. Mol. Genet. 15, 53–64.

Sevin, C., Verot, L., Benraiss, A., *et al*. (2007). Partial cure of established disease in an animal model of metachromatic leukodystrophy after intracerebral adeno-associated virus-mediated gene transfer. Gene Ther. 14, 405–414.

Sondhi, D., Hackett, N.R., Peterson, D.A., *et al*. (2007). Enhanced survival of the LINCL mouse following CLN2 gene transfer using the rh.10 rhesus macaque-derived adeno-associated virus vector. Mol. Ther. 15, 481–491.

Sondhi, D., Peterson, D.A., Edelstein, A.M., *et al*. (2008). Survival advantage of neonatal CNS gene transfer for late infantile neuronal ceroid lipofuscinosis. Exp. Neurol. 213, 18–27.

Souweidane, M.M., Fraser, J.F., Arkin, L.M., *et al*. (2010). Gene therapy for late infantile neuronal ceroid lipofuscinosis: Neurosurgical considerations. J. Neurosurg. Pediatr. 6, 115–122.

Takahashi, T., and Suzuki, T. (2012). Role of sulfatide in normal and pathological cells and tissues. J. Lipid Res. 53, 1437–1450.

Tuszynski, M.H., and Blesch, A. (2004). Nerve growth factor: From animal models of cholinergic neuronal degeneration to gene therapy in Alzheimer's disease. Prog. Brain Res. 146, 441–449.

von Figura, K., Gieselmann, V., and Jaeken, J. (2001). Metachromatic leukodystrophy. In *The Metabolic and Molecular Bases of Inherited Disease.* A.B. Scriver, A.R. Beaudet, W. Sly, and D. Valle, eds. (McGraw-Hill, New York), *pp.* 3695–3724.

Willingham, M.C., Pastan, I.H., Sahagian, G.G., *et al*. (1981). Morphologic study of the internalization of a lysosomal enzyme by the mannose 6-phosphate receptor in cultured Chinese hamster ovary cells. Proc. Natl. Acad. Sci. U.S.A. 78, 6967–6971.

Wittke, D., Hartmann, D., Gieselmann, V., *et al*. (2004). Lysosomal sulfatide storage in the brain of arylsulfatase A-deficient mice: Cellular alterations and topographic distribution. Acta Neuropathol. 108, 261–271.

Worgall, S., Sondhi, D., Hackett, N.R., *et al*. (2008). Treatment of late infantile neuronal ceroid lipofuscinosis by CNS administration of a serotype 2 adeno-associated virus expressing CLN2 cDNA. Hum. Gene Ther. 19, 463–474.

Zaiss, A.K., Muruve, D.A. (2008) Immunity to adeno-associated virus vectors in animals and humans: a continued challenge. Gene Ther 15, 808–816.

Address correspondence to:
Dr. Ronald G. Crystal
Department of Genetic Medicine
Weill Cornell Medical College
1300 York Avenue, Box 164
New York, NY 10065

E-mail: geneticmedicine@med.cornell.edu

Received for publication January 3, 2014;
accepted after revision May 31, 2014.

Published online: June 12, 2014.